HHS Public Access

Author manuscript

Circulation. Author manuscript; available in PMC 2022 August 17.

Published in final edited form as:

Circulation. 2021 August 17; 144(7): 539–555. doi:10.1161/CIRCULATIONAHA.121.053980.

Nanoparticle Delivery of STAT3 Alleviates Pulmonary Hypertension in a Mouse Model of Alveolar Capillary Dysplasia

Fei Sun, PhD[1], **Guolun Wang, PhD**[1], **Arun Pradhan, PhD**[1], **Kui Xu, MD**[1], **Jose Gomez-Arroyo, MD, PhD**[1,2], **Yufang Zhang, MS**[1], **Gregory T. Kalin, BS**[1,3], **Zicheng Deng, MS**[1,4], **Ronald J. Vagnozzi, PhD**[5], **Hua He, PhD**[3], **Andrew W. Dunn, PhD**[1,4], **Yuhua Wang, PhD**[6], **Allen J. York, BS**[5], **Rashmi S. Hegde, PhD**[6,7], **Jason C. Woods, PhD**[7,8], **Tanya V. Kalin, MD, PhD**[3,7], **Jeffery D. Molkentin, PhD**[5,7,9], **Vladimir V. Kalinichenko, MD, PhD**[1,3,6,7,*]

[1]Center for Lung Regenerative Medicine, Perinatal Institute, Cincinnati Children's Hospital Medical Center, Cincinnati, USA.

[2]Department of Internal Medicine, Section of Pulmonary and Critical Care, University of Cincinnati, Cincinnati, USA.

[3]Division of Pulmonary Biology, Cincinnati Children's Hospital Medical Center, Cincinnati, USA.

[4]The Materials Science and Engineering Program, College of Engineering and Applied Science, University of Cincinnati, Cincinnati, USA.

[5]Division of Molecular Cardiovascular Biology, Heart Institute, Cincinnati Children's Hospital Medical Center, Cincinnati, USA.

[6]Division of Developmental Biology, Cincinnati Children's Hospital Medical Center, Cincinnati, USA.

[7]Department of Pediatrics, University of Cincinnati, Cincinnati Children's Hospital Medical Center, Cincinnati, USA.

[8]Center for Pulmonary Imaging Research, Division of Pulmonary Medicine, Cincinnati Children's Hospital Medical Center, Cincinnati, USA.

[9]Howard Hughes Medical Institute, Cincinnati Children's Hospital Medical Center, Cincinnati, USA.

Abstract

Background: Pulmonary hypertension (PH) is a common complication in patients with Alveolar capillary dysplasia with misalignment of pulmonary veins (ACDMPV), a severe congenital disorder associated with mutations in the *FOXF1* gene. While the loss of alveolar

[*]**Correspondence to**: Vladimir V. Kalinichenko, Vladimir.Kalinichenko@cchmc.org, Center for Lung Regenerative Medicine and Division of Pulmonary Biology, Cincinnati Children's Hospital Medical Center, 3333 Burnet Avenue, Cincinnati, OH 45229.

Author contributions: F.S. and V.V.K., designed the study; F.S., A.P., Y.Z., Z.D., R.J.V., A.W.D., Y.W. and A.J.Y. conducted experiments; F.S., H.H., G.T.K., J.G.A., R.S.H., J.C.W., T.V.K. and J.D.M. analyzed the data and provided critical insights; K.X., generated embryonic stem cells and performed blastocyst complementation; G.W. conducted bioinformatic analysis; F.S., J.G.A. and V.V.K. wrote the manuscript with input from all authors.

DISCLOSURES

Authors of this manuscript have no conflicts of interest.

microvasculature causes PH in ACDMPV patients, it is unknown whether increasing neonatal lung angiogenesis could prevent PH and right ventricular (RV) hypertrophy.

Methods: We used echocardiography, RV catheterization, immunostaining and biochemical methods to examine lung and heart remodeling and RV output in *Foxf1*$^{WT/S52F}$ mice carrying the *S52F Foxf1* mutation (identified in ACDMPV patients). The ability of *Foxf1*$^{WT/S52F}$ mutant embryonic stem cells (ESCs) to differentiate into respiratory cell lineages *in vivo* was examined using blastocyst complementation. Intravascular delivery of nanoparticles with a non-integrating *Stat3* expression vector was used to improve neonatal pulmonary angiogenesis in *Foxf1*$^{WT/S52F}$ mice and determine its effects on PH and RV hypertrophy.

Results: *Foxf1*$^{WT/S52F}$ mice developed PH and RV hypertrophy after birth. The severity of PH in *Foxf1*$^{WT/S52F}$ mice directly correlated with mortality, low body weight, pulmonary artery muscularization and increased collagen deposition in the lung tissue. Increased fibrotic remodeling was found in human ACDMPV lungs. Mouse ESCs carrying the *S52F Foxf1* mutation were used to produce chimeras via blastocyst complementation and to demonstrate that *Foxf1*$^{WT/S52F}$ ESCs have a propensity to differentiate into pulmonary myofibroblasts. Intravascular delivery of nanoparticles carrying *Stat3* cDNA protected *Foxf1*$^{WT/S52F}$ mice from RV hypertrophy and PH, improved survival and decreased fibrotic lung remodeling.

Conclusions: Nanoparticle therapies increasing neonatal pulmonary angiogenesis may be considered to prevent PH in ACDMPV.

Keywords

Pulmonary hypertension; Alveolar capillary dysplasia; FOXF1; STAT3; Nanoparticle delivery system

INTRODUCTION

Alveolar capillary dysplasia with misalignment of pulmonary veins (ACDMPV) is a rare congenital disorder which requires lung transplantation early in life [1, 2]. Early onset of ACDMPV, rapidly progressing respiratory insufficiency, and poor availability of pediatric donor lungs greatly complicate clinical care for ACDMPV patients, leading to mortality before lung transplantation. There is an urgent clinical need for new therapeutic approaches for ACDMPV patients. ACDMPV is characterized by reduced capillary density in alveolar regions, hypertrophy of small pulmonary arteries, and misaligned and congested pulmonary veins, the latter of which represent abnormal anastomoses between pulmonary and bronchial circulations [1]. Pulmonary hypertension (PH) occurs in a vast majority of ACDMPV cases, exacerbating respiratory insufficiency and edema and leading to pulmonary hemorrhage and extensive lung remodeling [1, 3]. While the pathophysiology of PH in ACDMPV is not entirely clear, reduced capillary density, severe lung tissue hypoxia and aberrant arterial-venal anastomoses appear to be the major contributing factors to PH. Recent studies reported a subset of rare ACDMPV cases with a late onset of PH, prolonged survival and a mosaic pattern of vascular abnormalities in the lung tissue [4, 5], supporting a link between the loss of alveolar microvasculature and PH. Based on histological assessment of ACDMPV fetuses and lung biopsies, a paucity of pulmonary capillaries and misalignment of pulmonary veins occur before birth as a result of abnormal lung vascular development, whereas PH and

RV hypertrophy occur postnatally [1]. While the loss of alveolar capillaries precedes PH in ACDMPV, it remains unknown whether neonatal proangiogenic therapies can prevent or delay PH in ACDMPV patients.

Heterozygous copy-number variant deletions and point mutations in the Forkhead Box F1 (*FOXF1*) gene locus have been recently linked to ACDMPV [2, 3]. FOXF1, a transcription factor expressed in pulmonary endothelial cells, fibroblasts and their mesenchymal progenitors [6-9] , is essential for lung vascular development [10, 11] and lung repair after injury [12-15]. During lung development, FOXF1 stimulates formation of alveolar capillaries by regulating genes critical for VEGF, PDGF and NOTCH signaling pathways [6, 16]. *Foxf1*$^{-/-}$ mice exhibit embryonic mortality before the initiation of lung development due to vascular abnormalities in the yolk sac and allantois [17]. Mice heterozygous for the *Foxf1 null* allele (*Foxf1*$^{+/-}$) or the *S52F Foxf1* mutant allele (*Foxf1*$^{WT//S52F}$) develop the alveolar capillary dysplasia before birth [2, 18]. However, it is unknown whether these mice have PH.

Recently developed nanoparticle carriers have been used to deliver small molecule compounds, DNA expression vectors, and stabilized mRNAs into cells *in vivo*. Nanoparticle carriers have shown minimal toxicity and accelerated the development of novel therapies for human cancers, diabetes and chronic inflammatory disorders. We have recently developed polyethylenimine-(5) myristic acid/ poly (ethylene glycol)-oleic acid/ cholesterol (PEI_{600}-MA_5/PEG-OA/Cho) nanoparticles to deliver non-integrating cDNA expression vectors into endothelial cells for the purpose of improving neonatal lung angiogenesis [2, 19]. Delivery of *Foxf1* cDNA increased lung angiogenesis after neonatal hyperoxic injury [20], whereas delivery of *Stat3*, a direct transcriptional target of FOXF1, increased neonatal angiogenesis in *Foxf1*$^{WT//S52F}$ mutant mice [2]. While the nanoparticle treatment stimulated the development of alveolar capillaries by transiently activating endothelial proliferation [2, 20], it is unclear whether restoring the pulmonary microvascular network will be sufficient to prevent or decrease PH and RV hypertrophy in ACDMPV mice.

In this study, we used nanoparticle delivery of *Stat3* cDNA to demonstrate that increasing neonatal lung angiogenesis prevents PH and RV hypertrophy, increases arterial oxygenation, reduces lung remodeling and improves survival in *Foxf1*$^{WT//S52F}$ mutant mice that contain the *S52F Foxf1* ACDMPV mutation. Nanoparticle-based proangiogenic therapy may be considered for treatment of human ACDMPV.

MATERIALS AND METHODS

Ethics Statement

The data, analytic methods, and study materials will be made available upon request from the corresponding author of this manuscript to other researchers for purposes of reproducing the results or replicating the procedures [2, 20]. All animal studies were based on AAALAC guidelines and approved by the Institutional Animal Care and Use Committee of the Cincinnati Children’s Hospital.

Mice

C57BL/6 mice and CD1 mice for generating chimeras were purchased from Jackson laboratory. The *Foxf1*$^{WT//S52F}$ mouse line was generated and maintained in C57BL/6 x 129/J genetic background as described [2]. *Foxf1*$^{WT//S52F}$ mice were genotyped by PCR (Figure IA-B in the Supplement). The Primers for genotyping were: *Foxf1* +77/+94, GGCGGCCAGGCCATGGAC; *Foxf1* +112/+133, CACCAAGGCCAAGAAGACCAAC; *Foxf1* +334/+313, GATGAAGCACTCGTTGAGCGAC. Postnatal day 2 (P2) mice were i.v. injected (25μl) with nanoparticles carrying a CMV expression plasmid containing *Stat3* cDNA or an empty CMV vector (5μg) through the facial vein. Mice were examined at 1, 4 and 6 months of age. Measurements of arterial oxygenation were recorded for 10 min using MouseOx Plus (STARR Life Sciences) as described [21].

Transthoracic echocardiography and right heart catheterization

Echocardiography was performed in a blinded manner by the Cincinnati Childre´s Hospital Medical Center echocardiography core. Echocardiographic measurements were taken under spontaneous respiration using Visualsonics Vevo 2100 ultrasonography (Visual Sonics, Toronto, Canada) with 40-MHz transducer as previously described [22]. Diastolic and systolic dimensions, tricuspid annular plane systolic excursion (TAPSE), S wave, stroke volume (SV) and cardiac output (CO) were recorded on M-mode, B-mode and tissue-Doppler images. The pulmonary artery peak velocity was measured to calculate the ratio of pulmonary acceleration time (PAT) to pulmonary ejection time (PAT/PET). Right heart catheterization and measurements of right ventricular systolic pressure (RVSP) were performed using FTH-1211B-0018 catheter as described [23].

Histology and immunostaining

Paraffin sections (5μm) or cryosections (7μm) were used for histological staining with hematoxylin and eosin (H&E), Sirius red, Masson's trichrome, wheat germ agglutinin (WGA) conjugated with Alexa Fluor 488 (Sigma) or immunostaining with various antibodies as described [24-27]. Antibodies are listed in Table I in the Supplement. Heath-Edwards classification was used to evaluate the grade of pulmonary vascular remodeling [28]. Relative vascular wall thickness was determined as $(d_o–d_i)/d_o$ x 100% (d_o, external diameter; d_i, internal diameter) as described [29]. De-identified human lung sections from ACDMPV patients were obtained from the Baylor College of Medicine [2, 3]. Whole mount immunostaining was described in [21]. For co-localization experiments, secondary antibodies conjugated with Alexa Fluor 488, Alexa Fluor 594 and Alexa Fluor 647 (all from Invitrogen) were used as described [30, 31]. Fluorescence images were captured by a Nikon Ti-E inverted confocal microscope. Brightfield images were captured by a Zeiss Axioplan2 microscope. Mean linear intercept (MLI) length was quantified by Image J software as previously described [20, 32].

Measurements of collagen content

The collagen concentration in lung tissue (left lobe) was determined by Sircol Soluble Collagen Assay (S1000, Biocolor) as previously described [7]. Collagen content (mg) was

calculated according to a standard curve and was normalized to the weight (g) of each lung tissue sample.

Quantitative real-time PCR (qRT-PCR) and microarray analysis

RNA was isolated from lung or heart tissues using RNeasy micro kit (Qiagen). RNA samples were reverse-transcribed into cDNA by iScript Reverse Transcription Reagents (BioRad) [33, 34]. Samples were amplified using inventoried TaqMan primers (Applied Biosystems) listed in Table II in the Supplement. qRT-PCR was performed as previously described [35] using StepOnePlus Real-Time PCR system (Applied Biosystems). mRNAs were normalized to *β-actin* mRNA. The microarray data from donor and ACDMPV lungs (accession number GSE54780) were retrieved from the GEO database using GEOquery R package and analyzed by the R package limma software.

FACS analysis and Western blot

The single-cell suspension for flow cytometry was generated from enzyme-digested lung tissues as previously described [36, 37]. Viability of cells was > 90% as determined with 7-AAD or zombie-UV (eBioscience). Antibodies are listed in Table I in the Supplement. Cell fixation and permeabilization protocol for intracellular staining was described previously [38]. Isotype IgG were used as controls for intracellular staining. The data were acquired and analyzed using 5-laser LSRII (BD Biosciences). Western blotting of total lung protein extract was performed as described [2, 39].

Blastocyst complementation and generation of chimeras

Mouse embryonic stem cells (ESCs) containing the *S52F Foxf1* mutation and the *tdTomato* transgene (*tdT-S52F Foxf1 ESCs*) were generated using blastocysts from *Foxf1*$^{WT//S52F}$; *tdTomato*$^{tg/+}$ mice as described [21, 40]. *tdT-S52F Foxf1* ESCs and WT ESCs expressing *GFP* (*GFP-WT*) [21] were maintained *in vitro* for chimera generation. Male and female C57BL/6 mice were bred to produce blastocysts. Each blastocyst was injected with 16 donor ESCs (8 *tdT-S52F Foxf1* + 8 *GFP-WT*) using a piezo-assisted micromanipulator (Eppendorf). Chimeric blastocysts were transferred into the uteri of pseudopregnant recipient mice to continue normal embryonic development *in utero*. The chimera mice were sacrificed and analyzed at P7.

Nanoparticles

Polyethylenimine-(5) myristic acid/ poly (ethylene glycol)-oleic acid/ cholesterol (PEI_{600}-MA_5/PEG-OA/Cho) nanoparticles were synthesized as previously described [2, 19]. A mass ratio of 1:24 was used to encapsulate DNA (*CMV-Stat3* or *CMV-empty* plasmids) into polymers. Nanoparticle-DNA complexes were injected intravenously (i.v.) into P2 pups via the facial vein (25 μl total volume). The injection mixture contained 5 μg of plasmid DNA encapsulated into PEI_{600}-MA_5/PEG-OA/Cho nanoparticles (120 μg) as described [20].

Statistical analysis

Student's T-test and one-way ANOVA were used to determine statistical significance. The right skewed measurements were log-transformed to meet normality assumption prior to

analysis. Multiple means were compared using one-way analysis of variance with the post-hoc Tukey test. *P* values less than 0.05 were considered significant. For datasets with n<5, non-parametric Mann-Whitney U test was used to determine statistical significance. Values for all data were showed as the mean ± standard error of mean (SEM).

RESULTS

Foxf1$^{WT/S52F}$ mice exhibit right ventricular hypertrophy and pulmonary hypertension.

Since human ACDMPV is associated with PH [1], we examined whether *Foxf1*$^{WT/S52F}$ *knock-in* mice (containing the heterozygous *S52F Foxf1* mutation which is identical to those found in ACDMPV patients [2]) have PH. Right ventricular (RV) systolic pressure (RVSP) was increased in adult *Foxf1*$^{WT/S52F}$ mice compared to wild type (*WT*) littermates as shown by RV catheterization (Figure 1A). To compare the pulmonary vascular resistance, we used transthoracic echocardiography to measure the pulmonary acceleration time (PAT) and the pulmonary ejection time (PET) and calculated the PAT/PET ratio, a reliable indicator of pulmonary artery (PA) blood flow and RV function [22]. The PAT/PET ratio was decreased in adult *Foxf1*$^{WT/S52F}$ mice (Figure 1B-C), indicating higher PA pressure and worse RV function compared to *WT* littermates. Diastolic and systolic RV wall thickness and the RV chamber area were increased in *Foxf1*$^{WT/S52F}$ mice (Figure 1D and Figure IC in the Supplement). TAPSE, stroke volume, S wave and cardiac output were reduced (Figure 1E-H), consistent with impaired RV function in *Foxf1*$^{WT/S52F}$ mice. While interventricular septum (IVS), left ventricular (LV) mass and LV chamber dimensions were mostly similar between WT and *Foxf1*$^{WT/S52F}$ mice, diastolic LV internal diameter and diastolic LV volume were increased (Figure ID in the Supplement).

Foxf1$^{WT/S52F}$ hearts were enlarged and the heart weight to body weight ratio was increased compared to *WT* controls (Figure IIA-C in the Supplement). Histological examination of *Foxf1*$^{WT/S52F}$ hearts showed an increased thickness of RV walls (Figure 1I), and an increased ratio of RV weight to the combined weight of LV and interventricular septum (RV/[LV+S]) (Figure 1J), findings consistent with RV hypertrophy. Expression of cardiac hypertrophy genes *Nppa*, *Nppb* and *Myh7*, and the *Myh7/Myh6* ratio were increased in total RNA samples prepared from right ventricles of *Foxf1*$^{WT/S52F}$ mice (Figure IID-H in the Supplement). Based on wheat germ agglutinin (WGA) staining, the size of RV cardiomyocytes was increased in *Foxf1*$^{WT/S52F}$ hearts (Figure 1K-L), whereas the size of LV cardiomyocytes was unchanged (Figure II I-J in the Supplement). There was no fibrosis in *Foxf1*$^{WT/S52F}$ hearts as demonstrated by Sirius red staining (Figure IIK in the Supplement). Thus, the *S52F Foxf1* mutation causes right ventricular hypertrophy and pulmonary arterial hypertension in adult mice. Interestingly, FOXF1 is expressed in the lung but not in the heart tissue (Figure IIIA in the Supplement), suggesting that lung vascular abnormalities cause RV hypertrophy in *Foxf1*$^{WT/S52F}$ mice.

Foxf1$^{WT/S52F}$ mice exhibit alveolar remodeling and thickening of small pulmonary arteries.

PH is frequently associated with lung remodeling, including alveolar simplification, capillary dysplasia, small artery muscularization and excessive collagen depositions into perivascular and alveolar regions [1]. Since FOXF1 is expressed in pulmonary endothelial

cells and fibroblasts [2, 7], we examined lung remodeling in adult *Foxf1*$^{WT/S52F}$ mice with PH. Histological examination of *Foxf1*$^{WT/S52F}$ lungs showed diffuse pulmonary inflammation and alveolar simplification (Figure 2A), the latter of which was confirmed by measurements of the mean linear intercept (Figure 2B). Capillary density and expression of endothelial *Pecam1* and *Flk1* mRNAs were decreased in *Foxf1*$^{WT/S52F}$ lungs (Figure 2C-F). STAT3 and p-STAT3 proteins were also decreased as shown by Western blot (Figure IVA-D in the Supplement) and immunostaining (Figure IVE-F in the Supplement), findings consistent with transcriptional activation of the *Stat3* gene by FOXF1 [2]. Compared to *WT* controls, increased fibrotic deposition was evident in *Foxf1*$^{WT/S52F}$ mice as determined by Sirius red staining (Figure 2G-H), Sircol assay measurements of collagen content (Figure 2I), and qRT-PCR for *Col1a1*, *Col3a1* and *Vim* mRNAs (Figure 2J). Consistent with PH, pulmonary arteries were remodeled in *Foxf1*$^{WT/S52F}$ mice, showing thick smooth muscle layers and increased expression of αSMA protein and mRNA (Figure 2K-M). While pulmonary arteries of all sizes were remodeled (Figure IIIB-D in the Supplement), small arteries exhibited the highest degree of remodeling (Figure IIIE in the Supplement). *Vegfa* mRNA was increased in *Foxf1*$^{WT/S52F}$ lungs, whereas *Hif1a* mRNA was unaltered (Figure VA-F in the Supplement). Neither VEGFα nor HIF-1α were changed in the arterial wall (Figure VG-H in the Supplement). Thus, in addition to RV hypertrophy and PH, *Foxf1*$^{WT/S52F}$ mice exhibit alveolar simplification, decreased capillary density, fibrotic lung remodeling and thickening of pulmonary arteries.

Pulmonary vascular abnormalities precede right ventricular hypertrophy in *Foxf1*$^{WT/S52F}$ mice.

Published studies showed that *Foxf1*$^{WT/S52F}$ embryos exhibited alveolar capillary dysplasia and misalignment of pulmonary veins prior to birth, whereas the pulmonary artery thickening occurred postnatally [2]. To determine the timing of RV hypertrophy in *Foxf1*$^{WT/S52F}$ mice, we examined hearts of *Foxf1*$^{WT/S52F}$ embryos and juvenile mice. At embryonic day 17.5 (E17.5), histological structure, IVS and myocardial thickness in the right ventricle were normal in *Foxf1*$^{WT/S52F}$ hearts (Figure VI in the Supplement). Thus, the *S52F Foxf1* mutation does not cause RV hypertrophy before birth. After birth, *Foxf1*$^{WT/S52F}$ mice had low body weights compared to *WT* littermates and often died before weaning (Figure VIIA-B in the Supplement). The mortality rate in *Foxf1*$^{WT/S52F}$ mice progressively increased after birth, reaching 69.2% at P28 (Figure VIIA in the Supplement). Autopsy of the dead *Foxf1*$^{WT/S52F}$ pups showed RV hypertrophy (Figure VIIC-D in the Supplement). Based on body weights and arterial oxygenation at 4 weeks of age, *Foxf1*$^{WT/S52F}$ mice were subdivided into two groups: *L-Foxf1*$^{WT/S52F}$ and *H-Foxf1*$^{WT/S52F}$ (Figure 3A-B and Figure VIIIA in the Supplement). The *L-Foxf1*$^{WT/S52F}$ group included *Foxf1* mutant mice with decreased arterial oxygenation and body weights lower than 6 grams, whereas *H-Foxf1*$^{WT/S52F}$ mice had normal arterial oxygenation and body weights higher than 6 grams (Figure 3A-B).

Morphological examination revealed that *L-Foxf1*$^{WT/S52F}$ hearts were lighter compared to hearts of WT and *H-Foxf1*$^{WT/S52F}$ littermates (Figure VIIIB-C in the Supplement). However, the ratio of heart weight to body weight (HW/BW) in *L-Foxf1*$^{WT/S52F}$ mice was increased (Figure VIIID in the Supplement). *L-Foxf1*$^{WT/S52F}$ hearts had a thicker

myocardium and enlarged cardiomyocyte sizes in the right ventricle compared to hearts of *WT* and *H-Foxf1*$^{WT/S52F}$ littermates (Figure 3C-E). The RV/[LV+S] ratio in *L-Foxf1*$^{WT/S52F}$ mice was higher, whereas the RV/[LV+S] ratio in *H-Foxf1*$^{WT/S52F}$ mice was similar to *WT* controls (Figure 3F). Consistent with RV hypertrophy, *Nppa*, *Nppb* and *Myh7* mRNAs, *H19* lncRNA, and the *Myh7/Myh6* mRNA ratio were selectively increased in the right ventricles of *L-Foxf1*$^{WT/S52F}$ but not *H-Foxf1*$^{WT/S52F}$ mice (Figure IXA-F in the Supplement). Capillary density in the right ventricle was similar in *WT* and *Foxf1* mutant hearts as shown by immunostaining for endomucin (Figure XA-B in the Supplement). There was no evidence for cardiac fibrosis (Figure XC in the Supplement). In contrast to the right ventricle, the cardiomyocyte size in the left ventricle was unchanged among all groups of mice (Figure XD-E in the Supplement). Altogether, RV hypertrophy in *Foxf1*$^{WT/S52F}$ mice occurs postnatally and directly correlates with mortality, low body weight and decreased arterial oxygenation.

Right ventricular hypertrophy in *Foxf1*$^{WT/S52F}$ mice directly correlates with reduced density of alveolar capillaries and arterial wall muscularization.

Histological examination revealed alveolar simplification and emphysema in *Foxf1*$^{WT/S52F}$ mice at 4 weeks of age, which was more severe in the *L-Foxf1*$^{WT/S52F}$ compared to the *H-Foxf1*$^{WT/S52F}$ group (Figure 4A-B). Immunostaining for PECAM1 and Endomucin revealed a paucity of alveolar capillary networks in both groups of *Foxf1*$^{WT/S52F}$ mutant mice, with the decrease of capillary density being more severe in *L-Foxf1*$^{WT/S52F}$ mice (Figure 4C-F). *L-Foxf1*$^{WT/S52F}$ lungs exhibited the lowest numbers of endothelial cells with nuclear staining for p-STAT3 (Figures 4E and 4G), a critical transcriptional regulator of endothelial proliferation and a direct target of FOXF1 [2]. *Pecam1* and *Flk1* mRNAs were lower in *L-Foxf1*$^{WT/S52F}$ lungs compared to *H-Foxf1*$^{WT/S52F}$ and *WT* lungs (Figure 4H-I). Consistent with decreased alveolar capillary density and reduced arterial oxygenation, *L-Foxf1*$^{WT/S52F}$ lungs exhibited increased expression of hypoxia-associated genes [41], including *Vegfa*, *Binp3*, *Slc2a1* and *Epas1*, the latter of which encodes HIF-2α transcription factor (Figure XI in the Supplement). Interestingly, HIF-1α staining and *Hif1a* mRNA were unchanged in *L-Foxf1*$^{WT/S52F}$ lungs (Figures XIA and XIIA-C in the Supplement). Consistent with reduced capillary density, *L-Foxf1*$^{WT/S52F}$ lungs exhibited decreased endothelial cell proliferation in the early postnatal period as shown by FACS analysis of P7 lungs for CD31 (PECAM1) and Ki-67 (Figure XIII in the Supplement).

Alveolar capillary dysplasia leads to increased blood pressure in the pulmonary circulation, causing hyperextension of pulmonary arteries and subsequent muscularization of the arterial wall [1]. Consistent with the most severe decreases in alveolar capillary density, muscularization of pulmonary arteries occurred in *L-Foxf1*$^{WT/S52F}$ but not in *H-Foxf1*$^{WT/S52F}$ lungs (Figure 5A-B) and was associated with increased *Acta2* mRNA (Figure 5C). Pulmonary arteries of all sizes were remodeled in *L-Foxf1*$^{WT/S52F}$ mice but their lumens were not occluded (Figure XIVA-D in the Supplement). Proliferation of αSMA^{+} arterial smooth muscle cells and PDGFRα^{+} fibroblasts was increased in *Foxf1*$^{WT/S52F}$ lungs at P7 (Figure XVA-C in the Supplement), whereas proliferation of endothelial cells lining pulmonary arteries was unchanged (Figure XVD-E in the Supplement). Interestingly, FOXF1 was not expressed in arterial smooth muscle cells at either P7 or P28 (Figure

XVIA-B in the Supplement), supporting indirect effects of the *S52F Foxf1* mutation on arterial remodeling. Altogether, reduced capillary density and muscularization of pulmonary arteries directly correlate with decreased arterial oxygenation, RV hypertrophy, low body weight and mortality in *Foxf1*$^{WT/S52F}$ juvenile mice.

Human and mouse ACDMPV lungs exhibit fibrotic lung remodeling.

Excessive collagen depositions were observed in *L-Foxf1*$^{WT/S52F}$ lungs by Sirius red (Figure 5D-E) and Masson's trichrome staining (Figure 5F-G). Increased collagen amounts and elevated *Col1a1*, *Col1a2*, *Col5a2, Col3a1* and *Vim* mRNAs were found in *L-Foxf1*$^{WT/S52F}$ lungs by Sircol assay and qRT-PCR (Figure 5H-I). There was no lung fibrosis in WT and *H-Foxf1*$^{WT/S52F}$ littermates (Figure 5D-I). Consistent with the murine ACDMPV model, lung biopsies from ACDMPV patients showed increased collagen depositions in alveolar and perivascular regions (Figure 5J and Figure XVII in the Supplement). Compared to donor lungs, microarray analysis of whole lung RNA from human ACDMPV lungs (n=8) revealed increased expression of multiple ECM genes, including *COL1A1*, *COL1A2*, *COL5A2*, *COL6A1* and *FBN2* (Figure 5K and Figure XVIII in the Supplement), a finding consistent with fibrotic lung remodeling. Both human ACDMPV and mouse *L-Foxf1*$^{WT/S52F}$ lungs exhibited increased expression of *H19* lncRNA (Figure 5K and Figures XI and XVIII in the Supplement), which is associated with PH and RV dysfunction [42]. Thus, human and mouse ACDMPV lungs exhibited increased fibrotic remodeling.

The *S52F Foxf1* mutation promotes differentiation of lung myofibroblasts from embryonic stem cells.

Excessive collagen depositions in ACDMPV lungs can occur due to aberrant differentiation of PDGFRα$^+$ fibroblasts into myofibroblasts. Therefore, we used immunostaining for αSMA and PDGFRα (CD140a) to identify myofibroblasts in *Foxf1*$^{WT/S52F}$ and control lungs. The percentage of αSMA$^+$PDGFRα$^+$ myofibroblasts among PDGFRα$^+$ fibroblasts was increased in alveolar regions of *L-Foxf1*$^{WT/S52F}$ mice as determined by immunostaining of tissue sections (Figure 6A-B) and FACS analysis of enzyme-digested lung tissue (Figure XIX in the Supplement).

Next, we tested whether the *S52F Foxf1* mutation accelerates differentiation of lung myofibroblasts from pluripotent embryonic stem cells (ESCs) *in vivo*. ESCs containing the *S52F Foxf1* mutation and the *tdTomato* lineage marker (*tdT-S52F Foxf1* ESCs) were generated from *Foxf1*$^{WT/S52F}$; *tdTomato* transgenic mice. *tdT-S52F Foxf1* ESCs formed typical ECS cell colonies *in vitro* (Figure XXA in the Supplement), which were similar to previously established GFP-labeled *WT* ESCs (*GFP-WT* ESCs) [21]. To compare the ability of *tdT-S52F Foxf1* and *GFP-WT* ESCs to differentiate into respiratory cell lineages *in vivo*, we used a blastocyst complementation method. Equal amounts of *tdT-S52F Foxf1* and *GFP-WT* ESCs were injected into the same *WT* blastocysts and the chimeric embryos were transplanted into the uterus of surrogate *WT* females to undergo normal embryonic development (Figure 6C). Mouse chimeras were harvested at P7 and examined for donor-derived cells using *tdTomato* and *GFP* fluorescence. Donor ECS-derived GFP$^+$ and tdTomato$^+$ cells were abundant in the lung tissue of chimeric mice (Figure 6D and Figure XXB in the Supplement). Consistent with pluripotency of donor ESCs, FACS

analysis showed that both *tdT-S52F Foxf1* and *GFP-WT* ESCs efficiently contributed to multiple respiratory cell types (Figure 6E-F and Figure XXIA-D in the Supplement). Cells formed by the fusion of GFP^+ and $tdTomato^+$ progenies in the lung tissue were rare (Figure 6E-F and Figure XXIA-D in the Supplement). The contribution of *tdT-S52F Foxf1* ESCs to the myofibroblast cell lineage was higher compared to *GFP-WT* ESCs as shown by FACS analysis (Figure 6E-F) and immunostaining of chimeric lungs for αSMA and PDGFRα (Figure 6G-J). Contributions of *tdT-S52F Foxf1* and *GFP-WT* ESCs to pericytes, endothelial, epithelial and hematopoietic cell lineages in chimeric lungs were similar (Figure XXI in the Supplement). Thus, *S52F Foxf1* ESCs have a propensity to differentiate into pulmonary myofibroblasts in the neonatal lung. The *S52F Foxf1* mutation does not influence ESC differentiation to other respiratory cell types.

Nanoparticle delivery of *Stat3* cDNA prevents RV hypertrophy and decreases lung remodeling in *Foxf1*$^{WT/S52F}$ mice.

Published studies demonstrated that nanoparticle delivery of the FOXF1 downstream target gene, STAT3, directly into endothelial cells increased alveolar capillary density in *Foxf1*$^{WT/S52F}$ lungs during the early neonatal period [2]. To determine whether increased capillary density is sufficient to protect the *L-Foxf1*$^{WT/S52F}$ mice from PH later in life, we injected the PEI_{600}-MA_5/PEG-OA/Cho nanoparticles carrying either a non-integrating CMV-*Stat3* expression vector or a CMV empty vector into the facial vein of P2 pups and harvested the mice at P28 (Figure 7A-B). Consistent with published studies [2], nanoparticle delivery of STAT3 improved the capillary density (Figure XXIIA-B in the Supplement), increased the number of p-$STAT3^+$ endothelial cells (Figure XXIIC in the Supplement), and increased *Pecam1* and *Flk1* mRNAs in *Foxf1*$^{WT/S52F}$ lungs (Figure XXIID-E in the Supplement). Increased capillary density in STAT3-treated *Foxf1*$^{WT/S52F}$ lungs was associated with increased arterial oxygenation (Figure 7C), supporting an improvement in alveolar gas exchange. Since the PEI_{600}-MA_5/PEG-OA/Cho nanoparticles do not target smooth muscle cells [19], neither STAT3 nor p-STAT3 were changed in pulmonary artery smooth muscle cells after the nanoparticle treatment (Figures XXIII-XXIV in the Supplement).

Delivery of STAT3 was sufficient to prevent PH and RV hypertrophy in *Foxf1*$^{WT/S52F}$ mice as shown by RV catheterization (Figure 7D) and transthoracic echocardiography to determine the PAT/PET ratio (Figure 7E and Figure XXVA in the Supplement), RV thickness and internal diameter (Figure 7F), TAPSE (Figure 7G), stroke volume, S wave and cardiac output (Figure XXVB-D in the Supplement). Decreased RV hypertrophy after STAT3 delivery was also supported by measurements of RV/[LV+S] (Figure 7H-I), and WGA staining to determine the size of cardiomyocytes in the right ventricle (Figure XXVIA-B in the Supplement). Although the nanoparticles targeted endothelial cells of several organs with equal efficiency, capillary density in the right ventricle was unchanged (Figure XXVIIA-D in the Supplement). Nanoparticle delivery of STAT3 did not alter p-STAT3 staining and the percentage of $STAT3^+$ endothelial cells in the heart and liver tissues (Figure XXVIIIA-C in the Supplement). In the lung tissue of *Foxf1*$^{WT/S52F}$ mice, alveolarization and pulmonary artery remodeling were improved after nanoparticle delivery of STAT3 compared to an empty vector (Figures XXIXA-B and XXXA-C in

the Supplement). Nanoparticle delivery of STAT3 did not change expression of epithelial markers pro-SPC and T1α (Figure XXXI in the Supplement) but decreased fibrotic depositions in *Foxf1*$^{WT/S52F}$ lungs as demonstrated by Sirius red staining (Figure XXXIIA-B in the Supplement) and expression of pro-fibrotic genes in whole lung RNA (Figure XXXIIC in the Supplement). *Vegfa* mRNA was decreased to normal levels, whereas *Hif1a* mRNA was unchanged (Figure XXXIIIA-B in the Supplement). Body weights and lung sizes of STAT3-treated *Foxf1*$^{WT/S52F}$ mice were higher compared to *L-Foxf1*$^{WT/S52F}$ mice injected with nanoparticles containing an empty vector (Figures XXXIV and XXXVA in the Supplement). Finally, a single nanoparticle delivery of STAT3 at P2 decreased 4-week mortality in *Foxf1*$^{WT/S52F}$ mice compared to untreated mice or *Foxf1*$^{WT/S52F}$ mice treated with nanoparticles containing an empty vector (Figure XXXVB in the Supplement). Altogether, increasing alveolar capillary density at the early neonatal period through nanoparticle delivery of STAT3 was sufficient to increase arterial oxygenation, prevent PH and RV hypertrophy, decrease lung remodeling and improve survival in *Foxf1*$^{WT/S52F}$ mice.

DISCUSSION

Pathological findings in ACDMPV lungs include the paucity of the alveolar capillary network, abnormal positioning (misalignment) of pulmonary veins and global lung hypoplasia [1]. Altogether, these congenital lung abnormalities result in severe PH and fulminant respiratory failure shortly after birth [1]. While PH exacerbates this syndrome and contributes to high mortality rate, the pathophysiological mechanisms causing PH in ACDMPV remain unclear. In the present study, we demonstrated that *Foxf1*$^{WT//S52F}$ mice not only develop the salient features of ACDMPV but also pulmonary hypertension, as evidenced by increased RVSP, decreased pulmonary artery acceleration time, pulmonary artery muscularization, and RV hypertrophy and dilation. We also demonstrated that pulmonary vascular remodeling precedes the development of RV hypertrophy, and this change in RV weight was not secondary to increased cardiac fibrosis but occurred mostly due to an increase in cardiomyocyte mass. Our studies suggest the PH phenotype in the setting of ACDMPV can be prevented using a systemic administration of nanoparticles containing the STAT3 expression vector, which increases alveolar capillary density via activation of endothelial proliferation [2]. It is unlikely that the nanoparticle STAT3 therapy can correct the misalignment of pulmonary veins and lung hypoplasia since these defects occur early during lung development. Despite the expression vector delivered by the nanoparticles is active only for 7 days in the neonatal lung [20], increasing alveolar capillary density at the early neonatal period was sufficient to prevent PH, decrease RV hypertrophy and improve survival in *Foxf1*$^{WT//S52F}$ mice. Our studies raise a possibility of using proangiogenic pulmonary therapies in human ACDMPV either caused by the *S52F FOXF1* mutation or associated with decreased STAT3 signaling.

The pulmonary circulation is a low-pressure circulatory system both at rest and during exercise [43]. Up to 45% of the total pulmonary vascular resistance results from the alveolar wall capillaries. Therefore, the PH phenotype seen in *Foxf1*$^{WT//S52F}$ mice could be a consequence of abnormal development of alveolar microvasculature, similarly to other forms of PH that are associated with abnormal or incomplete lung development in bronchopulmonary dysplasia (BPD) and congenital diaphragmatic hernia (CDH).

Foxf1$^{WT//S52F}$ lungs did not have arterial luminal occlusions or plexiform-like lesions that characterize other forms of pulmonary hypertension in mice or rat models. Although the loss of the *FOXF1* enhancer can cause capillary hemangiomatosis/pulmonary veno-occlusive disease [44], we did not observe histological changes consistent with pulmonary capillary hemangiomatosis in *Foxf1*$^{WT//S52F}$ mice. Decreased alveolar capillary density in *Foxf1* mutant mice can lead to reduced arterial oxygenation and lung tissue hypoxia, directly contributing to pulmonary fibrosis, arterial wall remodeling and PH. Decreased PAT/PET ratio, significant RV hypertrophy, increased RVSP and RV chamber dilation are all consistent with chronically elevated RV afterload in *Foxf1* mutant mice. One limitation of our study is that we were unable to predict which *Foxf1* mutant mice will develop *L-Foxf1*$^{WT//S52F}$ or *H-Foxf1*$^{WT//S52F}$ phenotype at birth. It is possible that the nanoparticle treatment outcome may be influenced by skewed inclusion of mice destined to become *L-Foxf1*$^{WT//S52F}$ or *H-Foxf1*$^{WT//S52F}$ mice in the treatment groups. Heterogeneity of the phenotypes in *Foxf1* mutant mice can be a consequence of the hybrid C57BL/6 x 129/J genetic background, in which the *Foxf1*$^{WT//S52F}$ mouse line is maintained to avoid uniform mortality after birth. To better understand ACDMPV pathogenesis, it will be interesting to identify genetic modifiers influencing the ratio between *L-Foxf1*$^{WT//S52F}$ and *H-Foxf1*$^{WT//S52F}$ phenotypes in *Foxf1* mutant mice.

Despite decreased arterial oxygenation and increased hypoxia-associated *Vegfa, Binp3, Epas1* and *Slc2a1* transcripts in the lung tissue, expression of HIF-1α was unchanged in *Foxf1* mutant mice. Since multiple FOXF1-binding sites are present in the *Hif1a* promoter, it is possible that FOXF1 transcriptionally activates the *Hif1a* gene and that FOXF1 deficiency prevents the increased expression of HIF-1α during hypoxia. STAT3 is known to promote arterial remodeling and PH when upregulated in pulmonary artery smooth muscle cells [45]. However, we did not observe increased STAT3 and p-STAT3 in vascular smooth muscle cells. These results are consistent with published studies [19] demonstrating that the PEI_{600}-MA_5/PEG-OA/Cho nanoparticles do not target arterial smooth muscle cells after i.v. administration.

Several members of the Forkhead box (FOX) family of transcription factors have been implicated in the development of PH [46]. Expression of FOXM1 was increased in the lungs of patients with idiopathic pulmonary arterial hypertension [47], and FOXM1 stimulated smooth muscle cell proliferation and arterial remodeling in rodents [48]. Inhibition of FOXO1 in smooth muscle cells caused pulmonary vascular remodeling and spontaneous PH [49]. *FOXF1*, a causative gene for ACDMPV [3], is expressed in pulmonary endothelial cells and fibroblasts but is absent in the adult heart. Here we demonstrate that the *S52F Foxf1* mutation increases the number of pulmonary myofibroblasts in the alveolar walls and perivascular regions. Fibrotic lung remodeling in *Foxf1*$^{WT//S52F}$ mice can be explained by hypoxia due to decreased microvascular density. Alternatively, FOXF1 may influence lung myofibroblasts via cell autonomous mechanisms. Consistent with this hypothesis, myofibroblast-specific inactivation of *Foxf1* exacerbated lung fibrosis in a bleomycin-induced mouse model [7]. Since the *S52F Foxf1* mutation encodes transcriptionally inactive S52F FOXF1 protein [2] and the number of myofibroblasts is increased in *Foxf1*$^{WT//S52F}$ lungs, our studies suggest that FOXF1 inhibits myofibroblasts differentiation. Blastocyst complementation of WT embryos with *S52F Foxf1* mutant embryonic stem cells was

performed in these studies, directly supporting the increased ability of *S52F Foxf1* mutant cells to differentiate into myofibroblasts, even in the *WT* lung environment. In addition to inhibiting myofibroblast differentiation, FOXF1 may decrease production of collagens by pulmonary myofibroblasts. FOXF1 protein directly bound to active repressors of *Col1a2* and *Col5a2* genes [50], providing direct support for this concept.

In summary, nanoparticle-mediated *Stat3* gene therapy (performed after birth) ameliorated PH, decreased RV hypertrophy and increased survival of *Foxf1*$^{WT//S52F}$ mice. Improvements in pulmonary hemodynamics and RV remodeling were the result of reduction in vascular resistance due to an increase in alveolar capillary density after nanoparticle treatment. Our findings suggest that nanoparticle *STAT3* gene therapy could be considered for the treatment of fulminant PH in patients with ACDMPV.

Supplementary Material

Refer to Web version on PubMed Central for supplementary material.

ACKNOWLEDGMENTS

We thank Erika Smith for excellent editorial assistance.

SOURCES OF FUNDING

This work was supported by NIH Grants HL141174 (to V.V.K.), HL149631 (to V.V.K.), HL152973 (to V.V.K. and T.V.K.), HL132849 (to T.V.K.) and HL152094 (to R.S.H.).

Non-standard Abbreviations and Acronyms

ACDMPV
alveolar capillary dysplasia with misalignment of pulmonary veins

Acta2
actin alpha 2

αSMA
alpha smooth muscle actin

Binp3
BCL2 Interacting protein 3

BPD
bronchopulmonary dysplasia

CDH
congenital diaphragmatic hernia

CMV
cytomegalovirus

Col1a1

collagen type 1 alpha 1 chain

Col1a2
collagen type 1 alpha 2 chain

Col3a1
collagen type 3 alpha 1 chain

Col5a2
collagen type 5 alpha 2 chain

Col6a1
collagen type 6 alpha 1 chain

d_i
internal diameter

d_o
external diameter

Epas1
endothelial PAS domain protein 1

ESCs
embryonic stem cells

FBN2
fibrillin 2

Flk1
fetal liver kinase 1

FOXF1
forkhead Box F1

GFP
green fluorescent protein

H&E
hematoxylin and eosin

Hif1a
hypoxia inducible factor 1 subunit alpha

i.v.
intravenous

IVS
interventricular septum

IVS;d
interventricular septal thickness at diastole

IVS;s
interventricular septal thickness at systole

LA
left atrium

LV
left ventricular

LVID;d
left ventricular internal diameter at the end of diastole

LVID;s
left ventricular internal diameter at the end of systole

LV Mass
left ventricular mass

LVPW;d
left ventricular posterior wall thickness at the end of diastole

LVPW;s
left ventricular posterior wall thickness at the end of systole

LV Vol;d
left ventricular volume at the end of diastole

LV Vol;s
left ventricular volume at the end of systole

MLI
mean linear intercept

Myh6
myosin heavy chain 6

Myh7
myosin heavy chain 7

Nppa
natriuretic peptide A

Nppb
natriuretic peptide B

PA
pulmonary artery

PAT
pulmonary acceleration time

PDGFRα
platelet-derived growth factor Alpha

Pecam1
platelet and endothelial cell adhesion molecule 1

PEI_{600}-MA_5/PEG-OA/Cho
polyethylenimine-(5) myristic acid/ poly (ethylene glycol)-oleic acid/ cholesterol

PET
pulmonary ejection time

PH
pulmonary hypertension

RV
right ventricular

RVID
right ventricular internal diameter

RVSP
right ventricular systolic pressure

RV/[LV+S]
ratio of RV weight to the combined weight of LV and interventricular septum

Slc2a1
solute carrier family 2 member 1

Stat3
signal transducer and activator of transcription 3

SV
stroke volume

TAPSE
tricuspid annular plane systolic excursion

tdT
tdTomato

Vegfa
vascular endothelial growth factor A

Vim
vimentin

WGA
wheat germ agglutinin

WT
wild type

REFERENCES

1. Bishop NB, Stankiewicz P and Steinhorn RH. Alveolar capillary dysplasia. Am J Respir Crit Care Med. 2011;184:172–179. [PubMed: 21471096]
2. Pradhan A, Dunn A, Ustiyan V, Bolte C, Wang G, Whitsett JA, Zhang Y, Porollo A, Hu YC, Xiao R, et al.The S52F FOXF1 Mutation Inhibits STAT3 Signaling and Causes Alveolar Capillary Dysplasia. Am J Respir Crit Care Med. 2019;200:1045–1056. [PubMed: 31199666]
3. Dharmadhikari AV, Szafranski P, Kalinichenko VV and Stankiewicz P. Genomic and Epigenetic Complexity of the FOXF1 Locus in 16q24.1: Implications for Development and Disease. Curr Genomics. 2015;16:107–116. [PubMed: 26085809]
4. Edwards JJ, Murali C, Pogoriler J, Frank DB, Handler SS, Deardorff MA and Hopper RK. Histopathologic and Genetic Features of Alveolar Capillary Dysplasia with Atypical Late Presentation and Prolonged Survival. J Pediatr. 2019;210:214–219 e2. [PubMed: 30853201]
5. Towe CT, White FV, Grady RM, Sweet SC, Eghtesady P, Wegner DJ, Sen P, Szafranski P, Stankiewicz P, Hamvas A, et al.Infants with Atypical Presentations of Alveolar Capillary Dysplasia with Misalignment of the Pulmonary Veins Who Underwent Bilateral Lung Transplantation. J Pediatr. 2018;194:158–164 e1. [PubMed: 29198536]
6. Whitsett JA, Kalin TV, Xu Y and Kalinichenko VV. Building and Regenerating the Lung Cell by Cell. Physiol Rev. 2019;99:513–554. [PubMed: 30427276]
7. Black M, Milewski D, Le T, Ren X, Xu Y, Kalinichenko VV and Kalin TV. FOXF1 Inhibits Pulmonary Fibrosis by Preventing CDH2-CDH11 Cadherin Switch in Myofibroblasts. Cell Rep. 2018;23:442–458. [PubMed: 29642003]
8. Kim IM, Zhou Y, Ramakrishna S, Hughes DE, Solway J, Costa RH and Kalinichenko VV. Functional characterization of evolutionary conserved DNA regions in forkhead box f1 gene locus. J Biol Chem. 2005;280:37908–37916. [PubMed: 16144835]
9. Kalinichenko VV, Gusarova GA, Shin B and Costa R. The Forkhead Box F1 Transcription Factor is Expressed in Brain and Head Mesenchyme during Mouse Embryonic Development. Gene Expr Patterns. 2003;3:153–158. [PubMed: 12711542]
10. Bolte C, Whitsett JA, Kalin TV and Kalinichenko VV. Transcription Factors Regulating Embryonic Development of Pulmonary Vasculature. Adv Anat Embryol Cell Biol. 2018;228:1–20. [PubMed: 29288383]
11. Ustiyan V, Bolte C, Zhang Y, Han L, Xu Y, Yutzey KE, Zorn AM, Kalin TV, Shannon JM and Kalinichenko VV. FOXF1 transcription factor promotes lung morphogenesis by inducing cellular proliferation in fetal lung mesenchyme. Dev Biol. 2018;443:50–63. [PubMed: 30153454]
12. Bolte C, Flood HM, Ren X, Jagannathan S, Barski A, Kalin TV and Kalinichenko VV. FOXF1 transcription factor promotes lung regeneration after partial pneumonectomy. Sci Rep. 2017;7:10690. [PubMed: 28878348]
13. Cai Y, Bolte C, Le T, Goda C, Xu Y, Kalin TV and Kalinichenko VV. FOXF1 maintains endothelial barrier function and prevents edema after lung injury. Sci Signal. 2016;9:ra40. [PubMed: 27095594]
14. Kalinichenko VV, Zhou Y, Shin B, Beer-Stoltz D, Watkins SC, Whitsett JA and Costa RH. Wild Type Levels of the Mouse Forkhead Box f1 Gene are Essential for Lung Repair. Am J Physiol Lung Cell Mol Physiol. 2002;282:L1253–L1265. [PubMed: 12003781]
15. Kalin TV, Meliton L, Meliton AY, Zhu X, Whitsett JA and Kalinichenko VV. Pulmonary mastocytosis and enhanced lung inflammation in mice heterozygous null for the Foxf1 gene. Am J Respir Cell Mol Biol. 2008;39:390–399. [PubMed: 18421012]

16. Bolte C, Ren X, Tomley T, Ustiyan V, Pradhan A, Hoggatt A, Kalin TV, Herring BP and Kalinichenko VV. Forkhead box F2 regulation of platelet-derived growth factor and myocardin/serum response factor signaling is essential for intestinal development. J Biol Chem. 2015;290:7563–7575. [PubMed: 25631042]
17. Mahlapuu M, Ormestad M, Enerback S and Carlsson P. The forkhead transcription factor Foxf1 is required for differentiation of extra-embryonic and lateral plate mesoderm. Development. 2001;128:155–166. [PubMed: 11124112]
18. Kalinichenko VV, Lim L, Beer-Stoltz D, Shin B, Rausa FM, Clark J, Whitsett JA, Watkins SC and Costa RH. Defects in Pulmonary Vasculature and Perinatal Lung Hemorrhage in Mice Heterozygous Null for the Forkhead Box f1 transcription factor. Dev Biol. 2001;235:489–506. [PubMed: 11437453]
19. Dunn AW, Kalinichenko VV and Shi D. Highly Efficient In Vivo Targeting of the Pulmonary Endothelium Using Novel Modifications of Polyethylenimine: An Importance of Charge. Adv Healthc Mater. 2018;7:e1800876. [PubMed: 30398703]
20. Bolte C, Ustiyan V, Ren X, Dunn AW, Pradhan A, Wang G, Kolesnichenko OA, Deng Z, Zhang Y, Shi D, et al.Nanoparticle Delivery of Proangiogenic Transcription Factors into the Neonatal Circulation Inhibits Alveolar Simplification Caused by Hyperoxia. Am J Respir Crit Care Med. 2020;202:100–111. [PubMed: 32240596]
21. Wang G, Wen B, Ren X, Li E, Zhang Y, Guo M, Xu Y, Whitsett JA, Kalin TV and Kalinichenko VV. Generation of Pulmonary Endothelial Progenitor Cells for Cell-Based Therapy Using Interspecies Mouse-Rat Chimeras. Am J Respir Crit Care Med. 2021; Online ahead of print, doi: 10.1164/rccm.202003-0758OC.
22. McCulley DJ, Wienhold MD, Hines EA, Hacker TA, Rogers A, Pewowaruk RJ, Zewdu R, Chesler NC, Selleri L and Sun X. PBX transcription factors drive pulmonary vascular adaptation to birth. J Clin Invest. 2018;128:655–667. [PubMed: 29251627]
23. Wang Y, Pandey RN, York AJ, Mallela J, Nichols WC, Hu YC, Molkentin JD, Wikenheiser-Brokamp KA and Hegde RS. The EYA3 tyrosine phosphatase activity promotes pulmonary vascular remodeling in pulmonary arterial hypertension. Nat Commun. 2019;10:4143. [PubMed: 31515519]
24. Wang IC, Meliton L, Ren X, Zhang Y, Balli D, Snyder J, Whitsett JA, Kalinichenko VV and Kalin TV. Deletion of Forkhead Box M1 transcription factor from respiratory epithelial cells inhibits pulmonary tumorigenesis. PloS One. 2009;4:e6609. [PubMed: 19672312]
25. Wang X, Bhattacharyya D, Dennewitz MB, Zhou Y, Kalinichenko VV, Lepe R and Costa RH. Rapid Hepatocyte Nuclear Translocation of the Forkhead Box M1B (FoxM1B) Transcription factor Causes a Transient Increase in Size of Regenerating Transgenic Hepatocytes. Gene Expr. 2003;11:149–162. [PubMed: 14686788]
26. Bolte C, Zhang Y, Wang IC, Kalin TV, Molkentin JD and Kalinichenko VV. Expression of Foxm1 transcription factor in cardiomyocytes is required for myocardial development. PloS One. 2011;6:e22217. [PubMed: 21779394]
27. Ramakrishna S, Kim IM, Petrovic V, Malin D, Wang IC, Kalin TV, Meliton L, Zhao YY, Ackerson T, Qin Y, et al.Myocardium defects and ventricular hypoplasia in mice homozygous null for the Forkhead Box M1 transcription factor. Dev Dyn. 2007;236:1000–1013. [PubMed: 17366632]
28. Heath D and Edwards JE. The pathology of hypertensive pulmonary vascular disease; a description of six grades of structural changes in the pulmonary arteries with special reference to congenital cardiac septal defects. Circulation. 1958;18:533–547. [PubMed: 13573570]
29. Rol N, Timmer EM, Faes TJ, Vonk Noordegraaf A, Grunberg K, Bogaard HJ and Westerhof N. Vascular narrowing in pulmonary arterial hypertension is heterogeneous: rethinking resistance. Physiol Rep. 2017;5:e13159. [PubMed: 28320897]
30. Ustiyan V, Wert SE, Ikegami M, Wang IC, Kalin TV, Whitsett JA and Kalinichenko VV. Foxm1 transcription factor is critical for proliferation and differentiation of Clara cells during development of conducting airways. Dev Biol. 2012;370:198–212. [PubMed: 22885335]
31. Ustiyan V, Zhang Y, Perl AK, Whitsett JA, Kalin TV and Kalinichenko VV. beta-catenin and Kras/Foxm1 signaling pathway are critical to restrict Sox9 in basal cells during pulmonary branching morphogenesis. Dev Dyn. 2016;245:590–604. [PubMed: 26869074]

32. Xia H, Ren X, Bolte CS, Ustiyan V, Zhang Y, Shah TA, Kalin TV, Whitsett JA and Kalinichenko VV. Foxm1 regulates resolution of hyperoxic lung injury in newborns. Am J Respir Cell Mol Biol. 2015;52:611–621. [PubMed: 25275225]
33. Milewski D, Pradhan A, Wang X, Cai Y, Le T, Turpin B, Kalinichenko VV and Kalin TV. FoxF1 and FoxF2 transcription factors synergistically promote rhabdomyosarcoma carcinogenesis by repressing transcription of p21Cip1 CDK inhibitor. Oncogene. 2017;36:850–862. [PubMed: 27425595]
34. Milewski D, Balli D, Ustiyan V, Le T, Dienemann H, Warth A, Breuhahn K, Whitsett JA, Kalinichenko VV and Kalin TV. FOXM1 activates AGR2 and causes progression of lung adenomas into invasive mucinous adenocarcinomas. PLoS Genet. 2017;13:e1007097. [PubMed: 29267283]
35. Hoggatt AM, Kim JR, Ustiyan V, Ren X, Kalin TV, Kalinichenko VV and Herring BP. The transcription factor Foxf1 binds to serum response factor and myocardin to regulate gene transcription in visceral smooth muscle cells. J Biol Chem. 2013;288:28477–28487. [PubMed: 23946491]
36. Sun L, Ren X, Wang IC, Pradhan A, Zhang Y, Flood HM, Han B, Whitsett JA, Kalin TV and Kalinichenko VV. The FOXM1 inhibitor RCM-1 suppresses goblet cell metaplasia and prevents IL-13 and STAT6 signaling in allergen-exposed mice. Sci Signal. 2017;10: eaai8583. [PubMed: 28420758]
37. Ren X, Zhang Y, Snyder J, Cross ER, Shah TA, Kalin TV and Kalinichenko VV. Forkhead box M1 transcription factor is required for macrophage recruitment during liver repair. Mol Cell Biol. 2010;30:5381–5393. [PubMed: 20837707]
38. Ren X, Ustiyan V, Guo M, Wang G, Bolte C, Zhang Y, Xu Y, Whitsett JA, Kalin TV and Kalinichenko VV. Postnatal Alveologenesis Depends on FOXF1 Signaling in c-KIT(+) Endothelial Progenitor Cells. Am J Respir Crit Care Med. 2019;200:1164–1176. [PubMed: 31233341]
39. Pradhan A, Ustiyan V, Zhang Y, Kalin TV and Kalinichenko VV. Forkhead transcription factor FoxF1 interacts with Fanconi anemia protein complexes to promote DNA damage response. Oncotarget. 2016;7:1912–1926. [PubMed: 26625197]
40. Wen B, Li E, Ustiyan V, Wang G, Guo M, Na CL, Kalin GT, Galvan V, Xu Y, Weaver TE, et al.In Vivo Generation of Lung and Thyroid Tissues from Embryonic Stem Cells Using Blastocyst Complementation. Am J Respir Crit Care Med. 2021;203:471–483. [PubMed: 32877203]
41. Voelkel NF, Mizuno S and Bogaard HJ. The role of hypoxia in pulmonary vascular diseases: a perspective. Am J Physiol. 2013;304:L457–L465.
42. Omura J, Habbout K, Shimauchi T, Wu WH, Breuils-Bonnet S, Tremblay E, Martineau S, Nadeau V, Gagnon K, Mazoyer F, et al.Identification of Long Noncoding RNA H19 as a New Biomarker and Therapeutic Target in Right Ventricular Failure in Pulmonary Arterial Hypertension. Circulation. 2020;142:1464–1484. [PubMed: 32698630]
43. Naeije R and Chesler N. Pulmonary circulation at exercise. Compr Physiol. 2012;2:711–741. [PubMed: 23105961]
44. Dello Russo P, Franzoni A, Baldan F, Puppin C, De Maglio G, Pittini C, Cattarossi L, Pizzolitto S and Damante G. A 16q deletion involving FOXF1 enhancer is associated to pulmonary capillary hemangiomatosis. BMC Med Genet. 2015;16:94. [PubMed: 26462560]
45. Paulin R, Meloche J and Bonnet S. STAT3 signaling in pulmonary arterial hypertension. JAKSTAT. 2012;1:223–233. [PubMed: 24058777]
46. Stenmark KR, Hu CJ and Pullamsetti SS. How Many FOXs Are There on The Road to Pulmonary Hypertension? Am J Respir Crit Care Med. 2018;198:704–707. [PubMed: 29694238]
47. Dai Z, Zhu MM, Peng Y, Jin H, Machireddy N, Qian Z, Zhang X and Zhao YY. Endothelial and Smooth Muscle Cell Interaction via FoxM1 Signaling Mediates Vascular Remodeling and Pulmonary Hypertension. Am J Respir Crit Care Med. 2018;198:788–802. [PubMed: 29664678]
48. Bourgeois A, Lambert C, Habbout K, Ranchoux B, Paquet-Marceau S, Trinh I, Breuils-Bonnet S, Paradis R, Nadeau V, Paulin R, et al.FOXM1 promotes pulmonary artery smooth muscle cell expansion in pulmonary arterial hypertension. J Mol Med. 2018;96:223–235. [PubMed: 29290032]

49. Savai R, Al-Tamari HM, Sedding D, Kojonazarov B, Muecke C, Teske R, Capecchi MR, Weissmann N, Grimminger F, Seeger W, et al.Pro-proliferative and inflammatory signaling converge on FoxO1 transcription factor in pulmonary hypertension. Nat Med. 2014;20:1289–1300. [PubMed: 25344740]

50. Flood HM, Bolte C, Dasgupta N, Sharma A, Zhang Y, Gandhi CR, Kalin TV and Kalinichenko VV. The Forkhead box F1 transcription factor inhibits collagen deposition and accumulation of myofibroblasts during liver fibrosis. Biol Open. 2019;8:bio039800. [PubMed: 30670377]

CLINICAL PERSPECTIVE

What is new?

- *Foxf1*$^{WT/S52F}$ mice carrying the inactivating *S52F Foxf1* mutation (identified in ACDMPV patients) develop pulmonary hypertension and right ventricular hypertrophy which directly correlate with severity of lung remodeling in these mice.
- Pulmonary hypertension in *Foxf1*$^{WT/S52F}$ mice is secondary to alveolar capillary dysplasia, fibrotic lung remodeling and decreased endothelial expression of STAT3, a key downstream target of FOXF1 transcription actor.
- Nanoparticle delivery of STAT3 into the neonatal circulation prevents pulmonary hypertension and increases survival of *Foxf1*$^{WT/S52F}$ mice by improving alveolar microvascular networks and arterial oxygenation.

What are the clinical implications?

- Nanoparticle delivery of STAT3 may be considered for treatment of newborns and infants with ACDMPV associated with inactivating *FOXF1* mutations.
- Increasing neonatal lung angiogenesis may be considered for prevention of severe pulmonary hypertension and fulminant respiratory failure in patients with congenital lung diseases associated with abnormal or incomplete lung development.

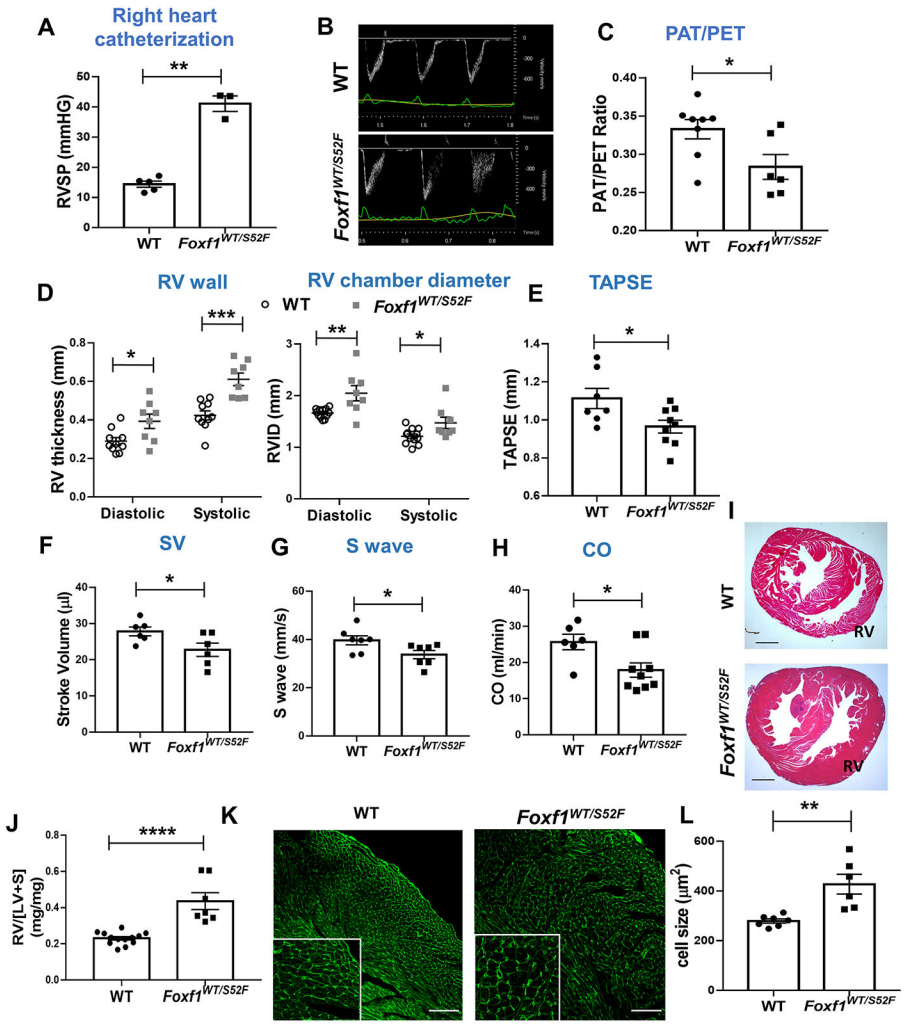

Figure 1. *Foxf1*$^{WT/S52F}$ mice develop right ventricular hypertrophy and pulmonary hypertension.

(A) Right heart catheterization shows increased RVSP in adult *Foxf1*$^{WT/S52F}$ mice compared to *WT* controls (n=3-5 mice per group). (B-C) Echocardiography shows a sharpened pulmonary artery velocity curve and a decreased ratio of pulmonary acceleration time (PAT) to pulmonary ejection time (PAT/PET) in adult *Foxf1*$^{WT/S52F}$ mice (n=6-8 mice per group). (D-H) *Foxf1*$^{WT/S52F}$ mice exhibit increased diastolic and systolic RV wall thickness and right ventricular internal diameter (RVID), whereas TAPSE, stroke volume (SV), S wave and cardiac output (CO) are decreased as determined by echocardiography (n=6-10 mice per group). (I) H&E staining of heart transverse sections shows increased thickness of RV walls in *Foxf1*$^{WT/S52F}$ mice. Scale bars are 2mm. (J) The ratio of right ventricle weight to the combined weight of left ventricle and interventricular septum (RV/[LV+S]) was determined after autopsy. RV/[LV+S] ratio is increased in *Foxf1*$^{WT/S52F}$ adult mice (n=7-13 mice per group). (K-L) Wheat germ agglutinin (WGA) staining of heart sections shows enlarged RV cardiomyocytes in *Foxf1*$^{WT/S52F}$ mice (n=6-7 mice per group). Scale bars are 100μm. * indicates $p < 0.05$, ** indicates $p < 0.01$, *** indicates $p < 0.001$, **** indicates $p < 0.0001$.

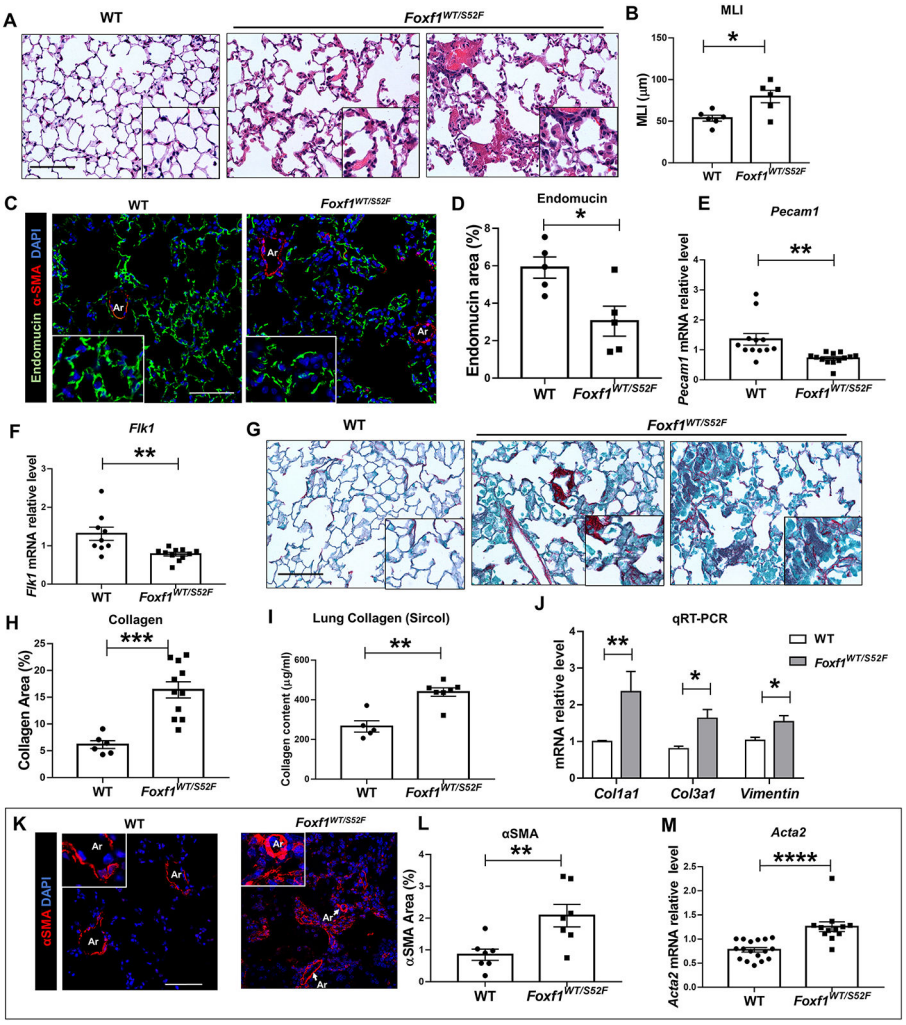

Figure 2. Adult *Foxf1*$^{WT/S52F}$ mice exhibit lung remodeling and vascular abnormalities.

(A-B) H&E staining of lung sections shows diffuse pulmonary inflammation and alveolar simplification in *Foxf1*$^{WT/S52F}$ adult mice. Mean linear intercept (MLI) was determined using 5 random images from each of 3 H&E-stained lung sections per mouse (n=6 mice). Scale bars are 50μm. (C-D) Immunostaining for Endomucin (green) and αSMA (red) shows reduced capillary density in lungs from *Foxf1*$^{WT/S52F}$ mice. Lung sections were counterstained with DAPI (blue). Five random lung images per mouse (n=5 mice per group) were used for quantification. Scale bars are 25μm. (E-F) qRT-PCR shows that *Pecam1* and *Flk1* mRNAs are decreased in *Foxf1*$^{WT/S52F}$ lungs. mRNAs were normalized using *β-actin* mRNA (n=9-13 mice per group). (G-H) Sirius red staining shows increased collagen deposition in *Foxf1*$^{WT/S52F}$ lungs. Scale bars are 50μm. Data were quantified using 5 random lung images per mouse (n=6-11 mice per group). (I) Sircol assay shows increased collagen content in the left lobe of *Foxf1*$^{WT/S52F}$ lungs (n=5-7 mice per group). (J) qRT-PCR shows that *Col1a1*, *Col3a1* and *Vimentin* mRNAs are increased in *Foxf1*$^{WT/S52F}$ lungs (n=6-9 mice per group). (K-L) Images show increased αSMA staining (red) with small artery muscularization (inserts) in lungs from *Foxf1*$^{WT/S52F}$ mice. Lung sections were counterstained with DAPI (blue). Data were quantified using 5 random lung images

per mouse (n=7 mice per group). Scale bars are 50μm. (M) qRT-PCR shows that *Acta2* mRNA is increased in lungs from *Foxf1*$^{WT/S52F}$ mice (n=12-17 mice per group). * indicates $p < 0.05$, ** indicates $p < 0.01$, *** indicates $p < 0.001$, **** indicates $p < 0.0001$. Abbreviations: MLI, Mean linear intercept; Ar, artery; V, vein.

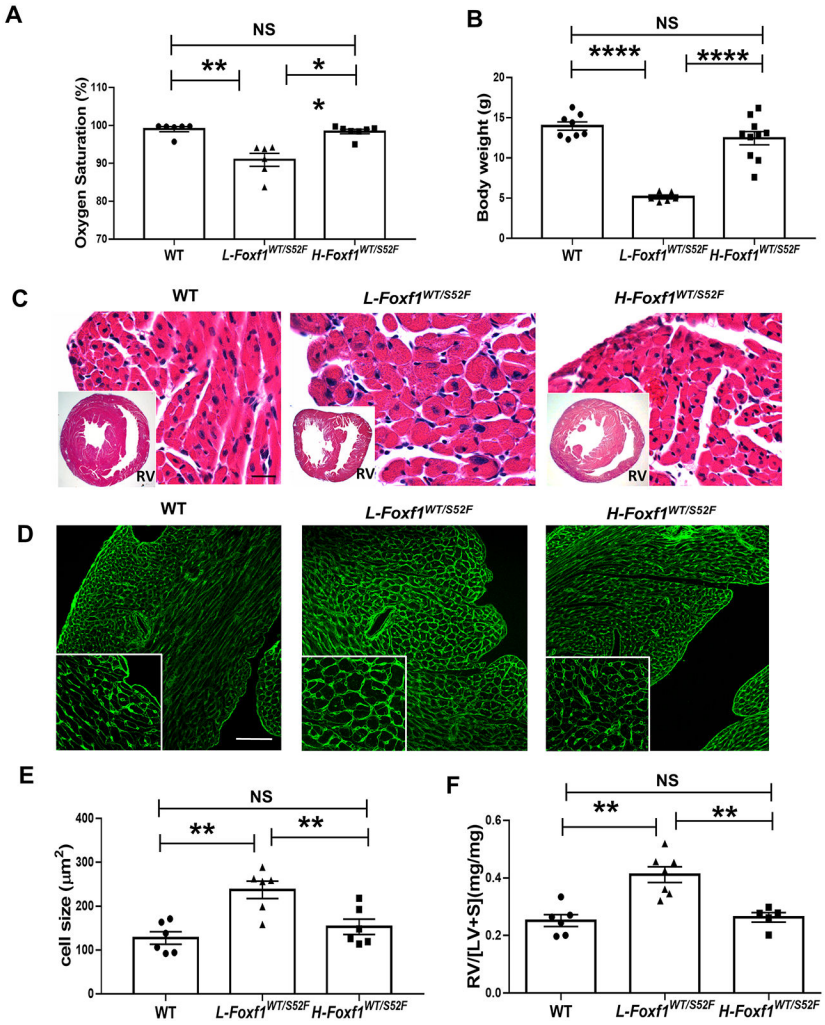

Figure 3. Low body weight in juvenile *Foxf1*$^{WT/S52F}$ mice is associated with right ventricular hypertrophy.

(A) Measurements of arterial oxygenation show decreased pO_2 in *L-Foxf1*$^{WT/S52F}$ mice compared to either *WT* or *H-Foxf1*$^{WT/S52F}$ littermates (n=6-7 mice per group). (B) Body weights are smaller in *L-Foxf1*$^{WT/S52F}$ mice compared to other groups (n=6-10 mice per group). (C) H&E staining of transverse heart sections shows histology and thickness of RV walls in *WT*, *L-Foxf1*$^{WT/S52F}$ and *H-Foxf1*$^{WT/S52F}$ littermates. Scale bars are 25μm. (D-E) Wheat germ agglutinin (WGA) staining of heart sections shows enlarged RV cardiomyocytes in *L-Foxf1*$^{WT/S52F}$ mice. Average cell size was determined using 5 random heart images per mouse (n=6 mice per group). Scale bars are 100μm. (D) Ratio of RV weight to the combined weight of LV and interventricular septum (RV/[LV+S]) is increased in *L-Foxf1*$^{WT/S52F}$ mice (n=5-7 mice per group). NS indicates no significance, ** indicates $p < 0.01$, **** indicates $p < 0.0001$.

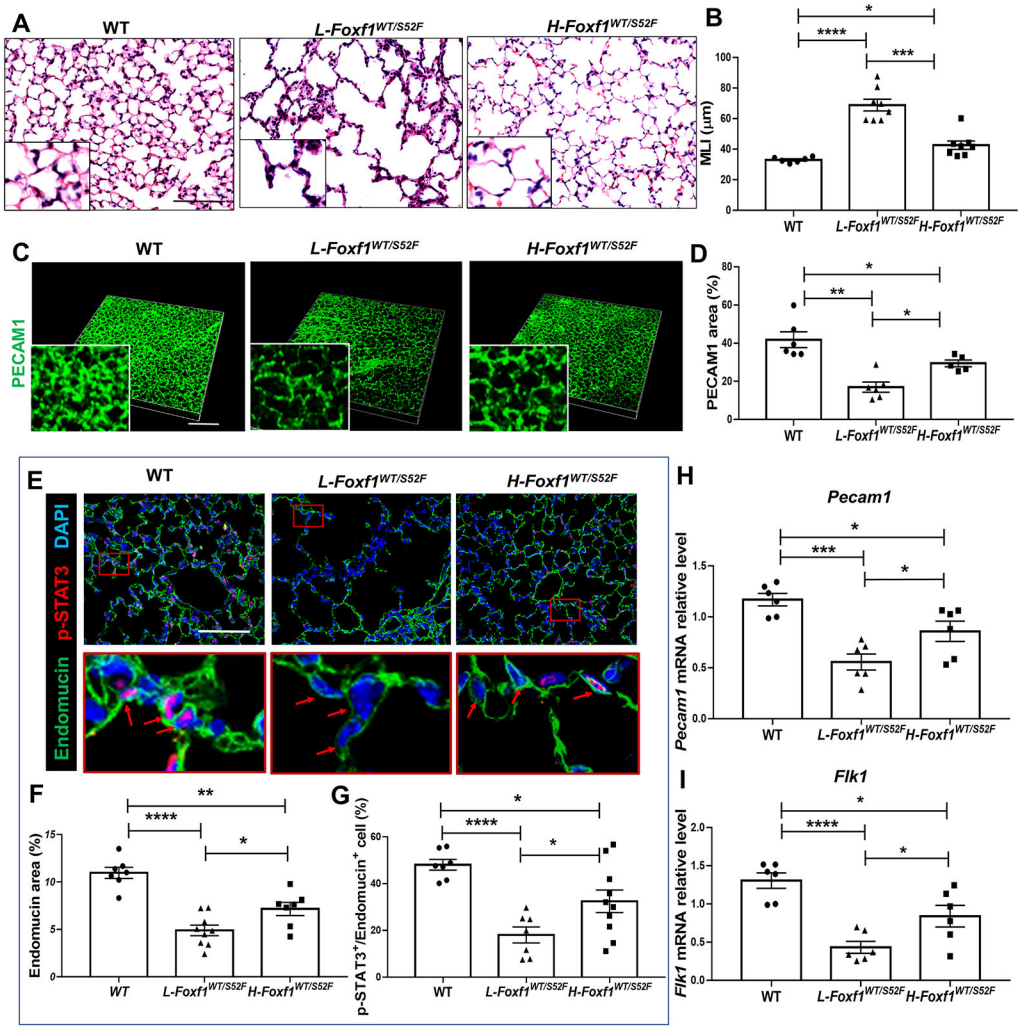

Figure 4. Low body weight in juvenile *Foxf1*$^{WT/S52F}$ mice is associated with alveolar capillary dysplasia and decreased p-STAT3.

(A-B) H&E staining of lung sections shows severe alveolar simplification in *L-Foxf1*$^{WT/S52F}$ mice. Mean linear intercept (MLI) was determined using 5 random images from each of 3 lung sections per mouse (n=6-8 mice per group). Scale bars are 50μm. (C-D) Whole mount PECAM1 immunostaining of lung slices shows decreased capillary density in *L-Foxf1*$^{WT/S52F}$ lungs. Data were quantified using 5 random lung images per mouse (n=5-6 mice per group). Scale bars are 100μm. (E-G) Immunostaining for Endomucin (green) and p-STAT3 (red) shows decreased capillary density and a decreased number of endothelial cells expressing p-STAT3 in *L-Foxf1*$^{WT/S52F}$ lungs. Bottom images show the area in red box. Arrows point to nuclei of endothelial cells. Slides were counterstained with DAPI (blue). Five random lung images per mouse were used to quantify the data (n=7-10 mice per group). Scale bars are 100μm. (H-I) qRT-PCR shows that *Pecam1* and *Flk1* mRNAs are decreased in total lung RNA from *L-Foxf1*$^{WT/S52F}$ mice. mRNAs were normalized using *β-actin* mRNA (n=6 mice per group). NS indicates no significance, * indicates $p < 0.05$, ** indicates $p < 0.01$, *** indicates $p < 0.001$, **** indicates $p < 0.0001$.

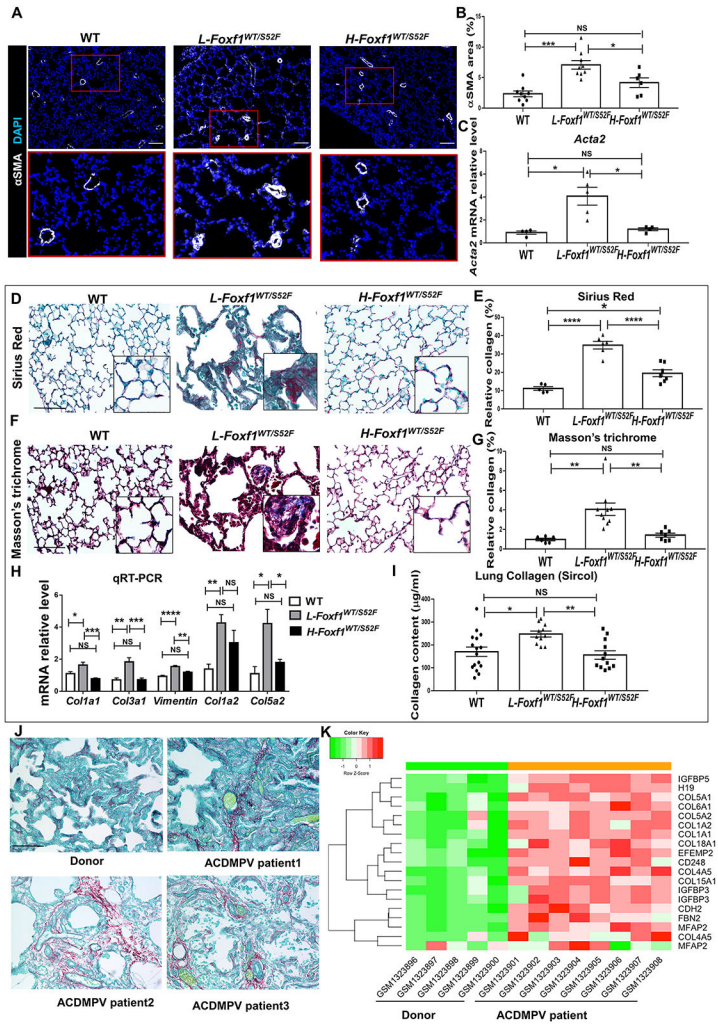

Figure 5. Human ACDMPV and mouse *L-Foxf1*$^{WT/S52F}$ lungs have increased collagen deposition.

(A-B) Immunostaining for αSMA shows muscularization of small lung arteries in *L-Foxf1*$^{WT/S52F}$ mice. Bottom images show the area in red box. Sections were counterstained with DAPI (blue). Data were quantified using 5 random lung images per mouse (n=6-9 mice per group). Scale bars are 100μm. (C) qRT-PCR shows that *Acta2* mRNA is increased in *L-Foxf1*$^{WT/S52F}$ lungs. *Acta2* mRNA was normalized using *β-actin* mRNA (n=4-5 mice per group). (D-E) Sirius red staining shows increased collagen deposition in *L-Foxf1*$^{WT/S52F}$ lungs (n=5-7 mice per group). Five random lung images per mouse were used to quantify collagen deposition. Scale bars are 50μm. (F-G) Masson's trichrome staining shows increased collagen deposition in *L-Foxf1*$^{WT/S52F}$ mice (n=6-10 mice per group). Scale bars are 50μm. (H) qRT-PCR shows that *Col1a1*, *Col3a1*, *Vimentin, Col1a2* and *Col5a2* mRNAs are increased in *L-Foxf1*$^{WT/S52F}$ lungs (n=6-13 mice per group). (I) Sircol assay shows increased collagen content in the left lobe of *L-Foxf1*$^{WT/S52F}$ lungs (n=11-16 mice per group). (J) Sirius red staining of lung biopsies shows increased collagen deposition in alveolar and perivascular regions of ACDMPV patients compared to donor lungs (n=3). Scale bars are 50μm. (K) Microarray analysis of whole lung RNA from ACDMPV patients

(n=8) shows increased expression of ECM genes compared to age-matched donor lungs (n=5). NS indicates no significance, * indicates $p < 0.05$, ** indicates $p < 0.01$, *** indicates $p < 0.001$, **** indicates $p < 0.0001$.

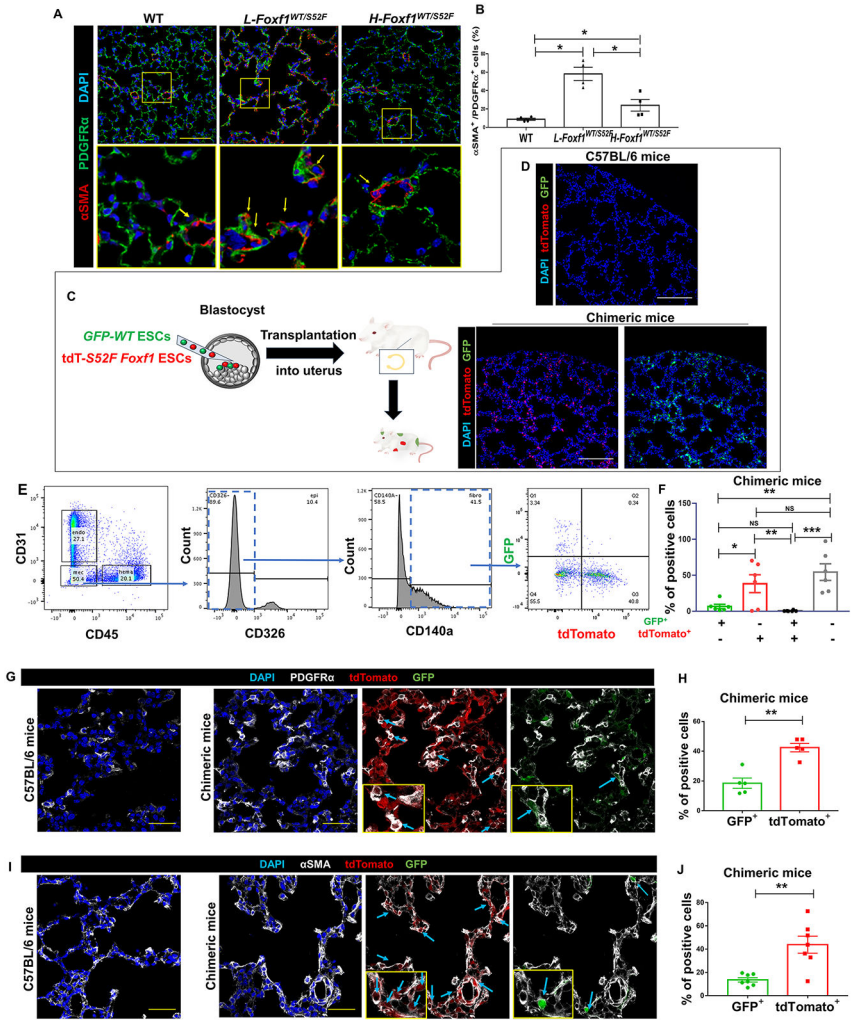

Figure 6. Embryonic stem cells with *S52F Foxf1* mutation have a propensity to differentiate into pulmonary myofibroblasts.

(A-B) Immunostaining shows an increased number of myofibroblasts co-expressing αSMA and PDGFRα in *L-Foxf1*$^{WT/S52F}$ lungs. Bottom images show the area in the yellow box. Sections were counterstained with DAPI (blue). Arrows point to αSMA^{+}PDGFRα^{+} myofibroblasts. The percentage of αSMA^{+}PDGFRα^{+} cells among PDGFRα^{+} fibroblasts in the alveolar region was counted using 5 random lung images per mouse (n=4-6 mice per group). Scale bars are 100μm. (C) Schematic diagram showing the injection of donor ESCs into mouse blastocysts and generation of chimeric mice. (D) Confocal images show contributions of donor *S52F Foxf1* ESCs expressing tdTomato (*tdT-S52F Foxf1* ESCs, red) and *WT* ESCs expressing GFP (*GFP-WT* ESCs) to the lung tissue of chimeric mice. Donor-derived cells are detected in DAPI-stained lung tissue sections. Scale bars are 100μm. (E-F) FACS analysis of enzymatically-digested lung tissue from chimeras shows higher contribution of *tdT-S52F Foxf1* ESCs to the myofibroblast cell lineage (CD140a^{+}CD31^{-}CD45^{-}CD326^{-}) compared to *GFP-WT* ESCs. Lungs were harvested at P7 (n=6). (G-J) Immunostaining of frozen lung sections shows higher contribution of *tdT-S52F Foxf1* ESCs (red) to αSMA^{+} and PDGFRα^{+} cells compared to *GFP-WT* ESCs

(green). Sections were counterstained with DAPI (blue). Arrows point to ESC-derived myofibroblasts. The percentage of ESC-derived myofibroblasts in the alveolar region was calculated using 5 random lung images per mouse (n=5-7 mice). Scale bars are 40μm. NS indicates no significance, * indicates $p < 0.05$, ** indicates $p < 0.01$, *** indicates $p < 0.001$.

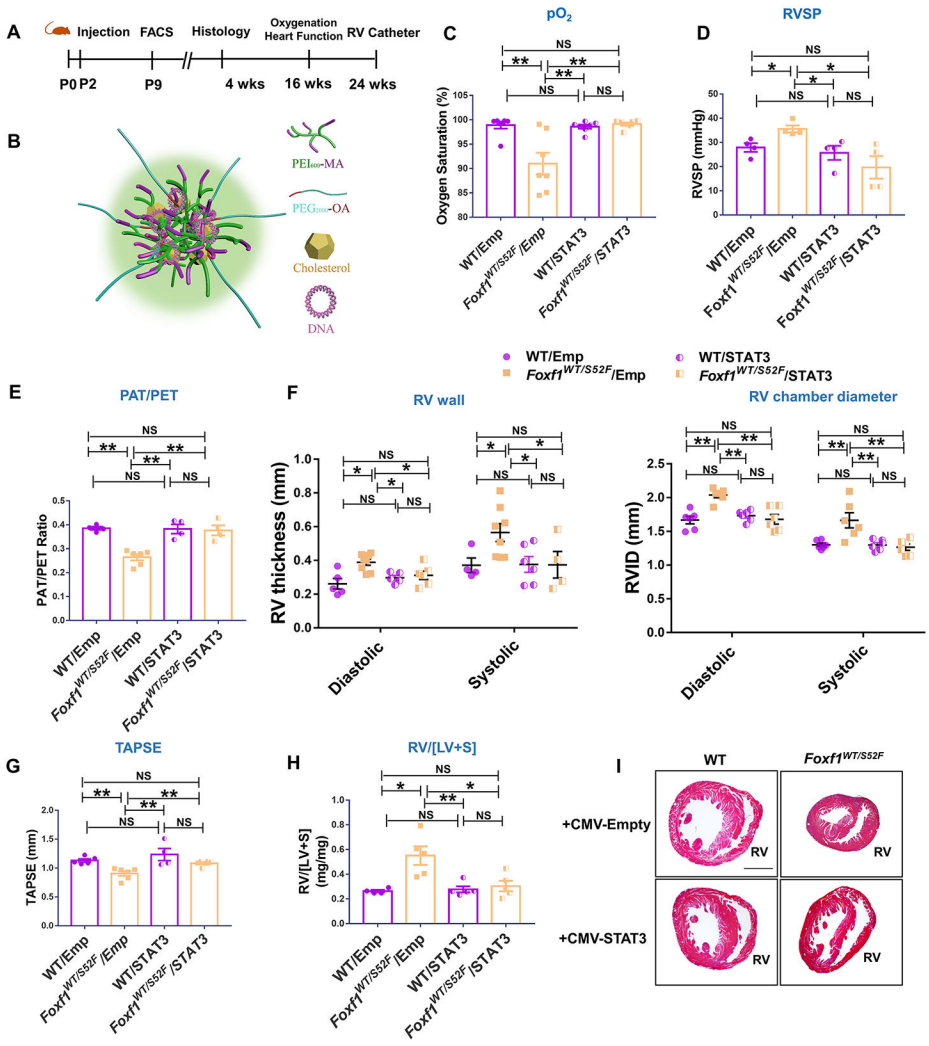

Figure 7. Nanoparticle delivery of *Stat3* cDNA prevents RV hypertrophy and increases survival of *Foxf1*$^{WT/S52F}$ mice.

(A) Schematic representation of nanoparticle treatment of *Foxf1*$^{WT/S52F}$ mice. Nanoparticle containing either *CMV-Stat3* (STAT3) or a CMV empty plasmid (Emp) were injected at P2 via the facial vein. FACS analysis was performed at P9. Histology and immunostaining were carried out at P28. Echocardiography and measurements of arterial oxygenation were performed at 4 months of age, whereas RV catheterization was performed at 6 months of age. (B) Schematic representation of nanoparticle structure shows PEI and PEG polymers, cholesterol and plasmid DNA. (C) Measurements of arterial oxygenation show that nanoparticle delivery of *Stat3* DNA increases pO_2 in *Foxf1*$^{WT/S52F}$ mice (n=7 mice per group). (D) STAT3 treatment decreases RVSP in *Foxf1*$^{WT/S52F}$ mice (n=4 mice per group). (E-G) Echocardiography shows improved ratio of pulmonary acceleration time (PAT) to pulmonary ejection time (PAT/PET) in *Foxf1*$^{WT/S52F}$ mice injected with STAT3 nanoparticles compared to CMV empty controls. Nanoparticle delivery of *Stat3* cDNA increases TAPSE but decreases diastolic and systolic RV wall thickness and the right ventricular internal diameter (RVID) in *Foxf1*$^{WT/S52F}$ mice (n=4-8 mice per group). (H) Nanoparticle delivery of *Stat3* cDNA decreases RV/[LV+S] in P28 *Foxf1*$^{WT/S52F}$ mice

(n=4-5 mice per group). (I) H&E staining shows transverse heart sections of *WT* and *Foxf1*$^{WT/S52F}$ mice that were either treated with STAT3 or control nanoparticles. Scale bars are 0.8mm. NS indicates no significance, * indicates $p < 0.05$, ** indicates $p < 0.01$. Abbreviations: RV/[LV+S], ratio of right ventricle weight to the combined weight of left ventricle and interventricular septum; RV, right ventricle; TAPSE, Tricuspid annular plane systolic excursion.